Quadrupole Levitation of Microscopic Dielectric Particles

ABSTRACT

Planar quadrupole microelectrodes, fabricated using surface micromachining, have been successfully used to achieve passive levitation of biological cells and other microscopic inorganic particles.
To explain certain experimental findings, namely the "size effect", a simple point charge quadrupole model was invoked to explain qualitatively the experimental observations. Subsequently, a more generalized multipolar theory was formulated to handle such higher order multipolar effects.
In this paper, we examine the salient properties of a practical planar quadrupole electrode structure as predicted by multipolar theory. The analytical data, obtained from multipolar theory is compared with the numerical modeling results from a boundary element simulation package and the levitation data of microscopic Spheriglass and polymethacrylate particles. The numerical simulation results and the levitation data are both consistent with and in good agreement with the predictions of multipolar theory.

Quadrupole Levitation of Microscopic Dielectric Particles

By

L. F. Hartley, K.V.I.S. Kaler and R. Paul*

Department of Electrical and Computer Engineering
University of Calgary
Calgary, Alberta
Canada (T2N-1N4)

***Department of Chemistry**
University of Calgary
Calgary, Alberta
Canada (T2N-1N4)

Corresponding Author: Karan V.I.S. Kaler

Abstract

Planar quadrupole microelectrodes, fabricated using surface micromachining, have been successfully used to achieve passive levitation of biological cells and other microscopic inorganic particles. To explain certain experimental findings, namely the "size effect", a simple point charge quadrupole model was invoked to explain qualitatively the experimental observations. Subsequently, a more generalized multipolar theory was formulated to handle such higher order multipolar effects.

In this paper, we examine the salient properties of a practical planar quadrupole electrode structure as predicted by multipolar theory. The analytical data, obtained from multipolar theory is compared with the numerical modeling results form a boundary element simulation package and the levitation data of microscopic Spheriglass® and polymethylmethacrylate particles. The numerical simulation results and the levitation data are both consistent with and in good agreement with the predictions of multipolar theory.

Introduction

Specially shaped non-uniform electric fields provide new and novel means of interrogation and manipulation of biological cells and other microscopic sized dielectric particles [1,2]. In particular, the techniques of dielectrophoresis (DEP) and electrorotation (ER) have been successfully applied to facilitate noninvasive "dielectric spectroscopy" of intact cells [3-6]. DEP/ER spectroscopy, of demonstrated value in cell research, provides an additional biophysical index for potential clinical diagnosis of cellular diseases [7-9]. In addition to cellular interrogation, DEP/ER have also been usefully applied in a variety of ways to manipulate microscopic particles [10,11] and macromolecules [12-14]. An important characteristic of recent DEP/ER experimentation is the novel use of planar surface micromachined electrode structures fabricated on insulating or semi-conducting substrates [15-19]. In this paper we examine performance of a surface micromachined planar quadrupolar levitator. The quadrupole structure is modeled using a 3-D boundary element electrostatics solver to determine the axial force profile of the levitator. The modeling results are compared with the analytical predictions obtained from multipolar theory and experimental levitation data, obtained on Spheriglass® and polymethylmethacrylate particles.

Quadrupolar levitation

DEP levitation of microscopic dielectric and conducting particles as well as biological cells has been demonstrated using cusped shaped electrostatic field realized by axis symmetric electrode configurations. Conventional DEP theory, is sufficient to model the behavior/performance of the levitator because the field induced DEP force is dominated by the dipolar interaction [20]. In this case, the DEP $\vec{F}_{DEP}$ force acting on a spherical

particle of radius r , relative permittivity ε_2 and conductivity σ_2 when suspended in a medium of relative permittivity ε_1 and conductivity σ_2 is as follows:

$$\vec{F}_{DEP} = (\vec{P} \bullet \nabla)\vec{E} = 2\pi r^3 \varepsilon_0 \varepsilon_1 \,\mathrm{Re}[\underline{K}_1]\nabla E^2 = 2\pi r^3 \varepsilon_0 \varepsilon_1 \,\mathrm{Re}\left[\frac{\underline{\varepsilon}_2 - \underline{\varepsilon}_1}{\underline{\varepsilon}_2 + 2\underline{\varepsilon}_1}\right]\nabla E^2 \qquad (1)$$

In Eqn. (1), $\vec{P}$ represents the equivalent induced dipole moment vector, $\vec{E}$ the applied electric field vector, $\varepsilon_0 = 8.854 \times 10^{-12}$ F m^{-1} is the permittivity of free space, $\underline{K}_1$ is the complex Clausius-Mossotti factor for the dipole . The quantities $\underline{\varepsilon}_1 = \varepsilon_1 - j\frac{\sigma_1}{\omega}$ and $\underline{\varepsilon}_2 = \varepsilon_2 - j\frac{\sigma_2}{\omega}$ are the complex relative permittivity of the medium and particle respectively, $\omega = 2\pi f$ is the radian frequency of the applied AC field and $j = \sqrt{-1}$.

This dipole approximation is not accurate when considering field induced interactions in highly non-homogenous fields because of induced higher order field interactions. Such cases can be handled readily by the new multipolar theory [21,22].

In quadrupole levitation, a dielectric particle is subjected to an quadrupolar electrostatic field, as realized by a system of four planar electrodes exhibiting azimuthal periodicity with the electrodes biased by alternate voltage sources (single-phase). According to the new theory, the dielectric particle will experience very different DEP force dependencies in the axial (z) and radial (ρ) directions, as shown in Equations (2a) and (2b) respectively [23].

Axial force:

$$F_Z = \frac{32\pi r^3 \varepsilon_0 \varepsilon_1}{3} \mathrm{Re}\left[\frac{\underline{\varepsilon}_2 - \underline{\varepsilon}_1}{2\underline{\varepsilon}_2 + 3\underline{\varepsilon}_1}\right]\left[a_2 b_2 + \left(b_2^2 + 12 a_2 c_2\right) z'\right] V^2 \qquad (2a)$$

$$= \frac{32\pi r^3 \varepsilon_0 \varepsilon_1}{3} \mathrm{Re}[\underline{K}_2]\left[a_2 b_2 + \left(b_2^2 + 12 a_2 c_2\right) z'\right] V^2$$

Radial force:

$$F_\rho = 16\pi\varepsilon_1 \left[r^3 \,\mathrm{Re}[\underline{K}_1] a_2^2 + \frac{2}{3} r^5 \,\mathrm{Re}[\underline{K}_2]\left(b_2^2 - 6 a_2 c_2\right)\right] V^2 \rho' \qquad (2b)$$

The quantities a_2, b_2, c_2 in Eqs. (2a) and (2b) are the coefficients whose values are electrode geometry specific. They may be obtained numerically or analytically, and they govern the precise characteristics of the planar quadrupole levitator. A more detailed discussion concerning the significance of these coefficients from a particle stability standpoint is given in [21].

The axial force expression F_z (Eqn. (2a)) includes the equilibrium term that balances the gravitational force. The z' and ρ' dependent terms in Eqn. (2a) and (2b) are respectively the perturbation forces acting on the particle as a result of a small axial and radial displacements from the equilibrium position. Axial stability of a negative DEP particle ($\underline{\varepsilon}_2 < \underline{\varepsilon}_1$) is ensured by an appropriately directed restoring force guaranteed by the condition $b_2^2 + 12a_2c_2 > 0$.

The absence of the conventional dipole DEP force term is readily apparent in Eqn. (2a). The axial force is determined instead by the quadrupole, which exhibits a stronger dependence on particle size (r^5) compared to the conventional dipole force (r^3) (Eqn. (1)). The radial force expression shows that, for a particle located on the central axis of the quadrupole field ($\rho = 0$), small radial excursions (ρ') about this equilibrium are countered by a restoring force that is influenced by both dipolar and quadrupole contributions.

Alternatively, equilibria and their stability may be computed analytically using the equivalent multipolar method if the quadrupolar electrostatic potential can be suitably modeled. Such an analysis has been described by Washizu et al [24]. In this analysis, the quadrupole is approximated by a system of 4 point charges (±Q) situated in the x-y plane and arranged symmetrically about the z-axis (see Fig. 1a). Assuming that the particle dimensions are small compared to the distance form the particle to the four point charges, the series expansion of the axial force component, in normalized form, is reasonably well approximated as follows:

$$\frac{F_z}{r^5} \cong -\frac{3Q^2}{\pi\varepsilon_0\varepsilon_1}\mathrm{Re}[\underline{K}_2]\frac{z/b}{b^7\left[1+(z/b)^2\right]^6} = \frac{3Q^2}{\pi\varepsilon_0\varepsilon_1}\mathrm{Re}[\underline{K}_2]G_{Quad}(z) \qquad (3)$$

where $G_{Quad}(z)$ represents all the geometric dependencies. The normalized force profile, Eqn. 3, for an ideal dielectric particle $(\varepsilon_2 = 4, \sigma_2 = 0, r = 1\mu m)$ suspended in an ideal dielectric medium $(\varepsilon_2 = 4, \sigma_2 = 0)$ is shown plotted in Fig.1b as a function of the normalized height (z/b) when subjected to a point charge quadrupole field ($Q = 1\mathrm{C}$, $b = 250\mu\mathrm{m}$).

Important characteristic features of the quadrupole levitator are revealed by examining the above force expression (Eqs. (1)-(3)) and analytical results obtained for the first order point charge quadrupole model (Fig. 1b). The magnitude, of both the radial and axial forces is proportional to Q2 or equivalently V^2 as expected of a DEP field effect. The force direction is influenced by the excess polarization terms $\underline{K}_1$, $\underline{K}_2$ and its sign depends on the relative magnitudes of $\underline{\varepsilon}_2$ and $\underline{\varepsilon}_1$. It is important to note that passive levitation of a dielectric particle is possible provided $\underline{K}_1$ and $\underline{K}_2$ are negative (i.e. negative DEP) and that the induced axial force opposes gravity. In such cases, the equilibrium levitation position is simply obtained by equating the axial component of induced DEP force to the opposing gravitational force (F_g) acting on the particle, as given in Eqn. (4).

$$\frac{3Q^2r^5}{\pi\varepsilon_0\varepsilon_1}\mathrm{Re}[\underline{K}_n]G_{Quad}(z) = F_g = \frac{4\pi r^3\rho g}{3} \qquad (4)$$

$$G_{Quad}(z) = \frac{4\pi^2\varepsilon_0\varepsilon_1\rho g}{9Q^2r^2\,\mathrm{Re}[\underline{K}_n]} \qquad (5)$$

where ρ is the medium density and $g = 9.81\ \mathrm{ms}^{-2}$

Since, the geometric function $G_{Quad}(z)$ exhibits local maxima above the plane of the source point charge quadrupole, there are two positions that satisfy Eqn. (4). However, stable

passive levitation is achieved only at the furthermost of the two equilibria, i.e. z values to the right of the maxima in Fig. 1b. Levitation at small axial displacements, to the left of the maxima, is only possible if some form of negative feedback control scheme is employed.

In the present work, we determine numerically the quadrupolar electrostatic field due practical planar quadrupole electrode and compute the body forces on model particles. Using a boundary element electrostatics solver, these findings are compared with the above analytical results obtained for the point charge quadrupole.

Planar Quadrupole Modeling

Numerical modeling of the structure was carried using a 3D boundary-element based electrostatic design package (Coulomb V2.6, Integrated Engineering Software, Winnipeg, Canada). Initially, the quadrupole structure was approximated by four spheres of radius 0.5 μm located at [(250 μm, 0, 0,), (0, 250 μm, 0) (-250 μm, 0, 0), (0, -250 μm, 0)] in the x-y plane as shown in Figure 1a. The spheres located on the x-axis each had imposed a total charge of −1C distributed uniformly over their surfaces, while the two spheres located on the y-axis each had a total charge of +1C. This numerical model allowed us to compare the numerical model results with the approximate point charge analytical model.

Five test particles of relative permittivity 4 and various radii were individually positioned along the z-axis of the structure at heights ranging from 5 to 30 μm in 5 μm increments and 30 to 300 μm in 10 μm increments. The net body force, acting on the test particles was computed numerically for each z-location. Since, the computation of the body force by the solver relies on the induced surface polarization charge and the field at the surface of the particle, both of which vary with particle location, required that the solver be run at each z-location. For comparison purposes, this numerical force was multiplied by $1/r^5$ and normalized to the peak analytical force corresponding to the maxima of the theory plot in Fig.1b, obtained using Eqn. (3) with (z/b) = $(1/11)^{0.5}$ [4]. The result of the transformation is shown in Fig. 2, plotted versus the normalized vertical height (z/b). Good agreement is obtained between theory and numerical data over wide range of normalized axial displacements.

After confirming the accuracy of the numerical solver, we turned our attention to the discrete planar quadrupole to address the degree to which a planar electrode structure emulates a point change quadrupole. Again, we examined the DEP force on a variety of spherical objects over a range of heights above the center of the discrete planar quadrupole surface. Sample results of such an analysis for 1 μm glass beads (Spheriglass®) are shown in Fig. 2. The force profile is almost identical to that of the analytical point charge model. This clearly confirms that the discrete planar quadrupole force profile may be modeled adequately by an equivalent point charge quadrupole. To determine the best fit equivalent point charge quadrupole, the discrete planar electrode generation was biased at 1V and a 1 μm radius particle of permittivity $\varepsilon_2 = 6.9$ translated from a height of 5 to 250 μm above the center of the quadrupole region. At each height, the electrostatic solver was run and the body force on the particle was numerically computed.

Optimization of the parameters b and q in the point charge quadrupole force equation (Eqn. (3)) was now possible. The point charge spacing b was adjusted to achieve the best fit of the equivalent analytical force profile to the numerical result. The magnitude of the equivalent point charge (q) was then set to equate the maximum of the analytical function (Eqn. 3) to the maximum value yielded by the field solver. This procedure yielded the optimal values for the equivalent point charge quadrupole with $q = 2.76 \times 10^{-13}$ C and $b = 124\,\mu$m. An alternative approach, to determine the equivalent dipole parameters, perhaps more directly, is to compute the field (or potential) due the planar quadrupole and than expand this field (or potential) in spherical harmonics to obtain numerical values for b and q .

Experimental Method

To verify, the characteristic force profile of a practical discrete planar quadrupole electrode structure, a quadrupole fluid integrated circuit was fabricated and assembled as shown in Fig. 3. The levitation chamber is comprised of a 40-pin integrated circuit carrier housing the quadrupole chiplet. The electrode structure on the chiplet was surface micromachined using conventional IC processing metal deposition and patterning technology. The substrate material in this case was 500 μm thick quartz glass upon which unpassivated chrome-gold electrodes were patterned (Fig. 4). Electrical contact to the four quadrupole chiplet pads and chip carrier bond pads was made using gold bonding wire and conductive epoxy (Circuit Works 2400). The chamber housing itself was machined out of Lucite® plastic fitted with horizontal view ports. To facilitate particle injection, a glass microtubule (1 mm OD and ~ 150 μm ID) was bonded to the vertical shaft drilled into the surface of the camber cavity. The Lucite® block was then carefully positioned and aligned, such that the microtubule tips was centered along the vertical axis of the quadrupole electrodes and positioned approximately 500 μm above the chiplet surface. The Lucite® block, once appropriately positioned was secured to the chip carrier using Silastic sealant. To complete the chamber assembly, 4mm long 16-gauge needles were epoxied into the chambers three primary fluid ports. The assembled chamber was mounted horizontally on a 2-axis microscope stage and the fluid ports connected to the fluid circuit as shown in Fig. 3. Before levitation experiments, the chamber was flushed several times with water of known conductivity to eliminate air bubbles. Individual test particles were introduced at the injection tube and made available for

experiments by introducing a dilute sample of washed test particles into the fluid circuit at port A and pumping fluid through the chamber at low flow rates (~10μm/min).

Particles, in the vicinity of the quadrupole electrodes were monitored by a B/W video camera (Javelin) coupled to a microscope. The video signal, from the camera was simultaneously fed to a real-time frame grabbing (Matrox MVP-AT Imager), recording (Panasonic) and display hardware (28" B/W monitor).

Separate, inverted and non-inverted phases of 100 kHz AC voltages were used to drive the planar quadrupole electrodes and made available by a signal generator (Hewlett Packard 8116 Function Generator). The magnitude of the applied voltage was manually controlled and monitored by a R.M.S. meter (Data Precision 3500).

Results

In the experiment we sought to confirm the r^5 dependence in the quadrupole DEP force expression and demonstrate the utility of the boundary element electrostatic simulator as a tool for integrated DEP system design. The above objectives were addressed experimentally by monitoring the axial location of a levitated particle as a function of the square of the applied quadrupole voltage. Two different microscopic dielectric particles, Spheriglass® and polymethylmethacrylate beads were selected for the experiments. The specific physical properties of these model particles are given in Table 1. The relative permittivity (ε_2) and density (ρ) values of the particles were provided by the manufacturer (Bangs Laboratories, Inc, Carmel, Indiana ,USA). The numerical value of the excess polarization term (K_2), as defined in Eqn. 2, was calculated using the respective particle permittivity data and a relative medium permittivity $\varepsilon_1 = 80$.

In a typical experimental run, a given spherical particle of known size was passively levitated at different axial locations above the planar quadrupole (see Fig. 5) and the applied rms. voltage squared was recorded. To facilitate direct comparison to the prediction of our model, the raw data was normalized. Typical normalized data for Spheriglass® particles in the size range $26.5 \leq R \leq 35.2$ are shown Fig. 6a together with the levitation force profile expected of equivalent charge quadrupole. There is reasonably good agreement between theory and experiment. As expected, stable passive levitation was achieved for axial distances $z > 35$ μm. The upper limit on z of 95 μm was imposed by joules heating and the onset of convective flow between adjacent electrodes, where both the field and potential gradients are the highest. In the central section of the chamber the flow patterns were directed upwards and radially outwards above the electrodes and observed to be symmetrical about the central

vertical axis of the chamber. The flow in the central section of the chamber, was however, not as pronounced as that observed near the electrodes. These observations are similar to those reported by Müller et al [17]. It should be noted that joules heating is not the only cause, responsible for the discrepancy between the modeling and experimental data. The axial force due to the quadrupole varies as r^5 and hence even small errors (~1%) in the measured values of r can result in sizable error (~5%) in the axial force. Furthermore, the modeling results, shown in Fig. 6a and Fig. 6b, were obtained for an ideal dielectric particle immersed in an ideal media (i.e. the particle conductivity and medium contribution were neglected in the force calculation). It is possible that such an approximation may also contribute to the observed discrepancy due to surface charging effects being present in practical particles at the measurement frequency. A more detailed modeling and experimental investigation is necessary in order to quantify such effects. In addition to the above, it is also possible that the higher order multipolar force contributions, not taken into account in the modeling results, are present in the experimental levitation data.

Normalized data for polymethylmethacrylate spheres is presented in Fig. 6b, together with the model predictions. Since, these polymer particles are less dense than Spheriglass® beads, stable levitation was attained at larger axial displacements for the same applied voltage range. The polymethylmethacrylate normalized data again confirm the modeling results for these particles.

As a test of the quadrupolar theory, it is useful to use the levitation data to extract the radius particle radius. Under stable passive DEP levitation conditions, the axially directed DEP (Eqn. 2a) induced by the quadrupolar electrostatic field is equal to the constant gravitational

force and hence, the radius(r) of particle levitated at any position z may be determined as follows:

$$r = \left[\frac{F_g}{\frac{32\pi\varepsilon_0\varepsilon_1}{3}\mathrm{Re}[\underline{K}_2][a_2 b_2]V^2} \right]^{\frac{1}{5}} = \left[\frac{\frac{F_g}{\left(\frac{F_g}{r^3}\right)}}{\left(\frac{F_{LEV}}{r^5 V^2}\right)V^2} \right]^{\frac{1}{5}} = \text{constant}$$

Where, $\left(\frac{F_g}{r^3}\right)$ is the gravitational force acting on a 1μm sized particle and $\left(\frac{F_{LEV}}{r^5 V^2}\right)$ is the normalized levitation force acting on a r = 1μm particle, where the planar electrodes are biased by ± 1V sources (as shown in Figs. 6a and 6b). Thus, the particle radius may be extracted from the levitation data obtained at various levitation positions provided the electrode geometry coefficients a_2, b_2 and the Clausius-Mossotti factor $\mathrm{Re}[\underline{K}_2]$ are known quantities and V^2 is determined experimentally, at each levitation height. In this investigation, we extracted the radius (r_{ext}) by appropriately transforming the characteristic ± 1V, 1 μm data and gravitational force, as shown above. Ideally, as a result of such a transformation, the extracted radius versus levitation height plot for particles of differing size should yield a family of horizontal (parallel to the x-axis,) line plots, located appropriately along the y-axis at the respective radii. The results of such a radius extraction carried out on the Spheriglass® and polymethylmethacrylate levitation data is shown in Fig. 7a and Fig. 7b respectively. The polymethylmethacrylate data, does indeed, exhibit the trend predicted ideally over an appreciable range of axial displacement (z) and the extracted radius is in good agreement with the measured values. However, at the larger axial distances the transformed data exhibits significant departure from the ideal straight horizontal line plots and the extracted and measured radii values differ significantly (12%). It is also interesting to note that for the

larger sized particles the extracted radius values are consistently larger than the actual measured value. Such a departure from the ideal behavior is observed to be more pronounced for the higher permittivity and density Spheriglass® beads (see Table 1). We suggest, that this may be attributed to an increase in joules heating since the levitation of the Spheriglass® particles at a given height requires much higher electrode voltages compared to the levitation of the similarly sized polymethylmethacrylate particles. As mentioned earlier, joules heating is most prominent in the high field regions between neighboring electrodes. At the highest voltages, typically 30 to 40 V_{rms}, such non-uniform heating effects are observed to give rise to convective fluid motion over an appreciable portion of the chamber.

Acknowledgements

The authors are grateful for the financial support received form NSERC in the form of operating grants to K.V. I. S. Kaler and R. Paul and an industrial fellowship to L.F. Hartley. The authors also acknowledge the very helpful discussions with T.B. Jones concerning DEP levitation.

References

1. H.A. Pohl, Dielectrophoresis, Cambridge University Press, Cambridge, 1978.
2. T.B. Jones, Electromechanics of particles, Cambridge University Press, Cambridge, 1995.
3. W.M. Arnold and U. Zimmermann, "Electro-rotation development of a technique for dielectric measurements on individual cells and particles", J. Electrostatics, 21(1988) 151-191.
4. K.V.I.S. Kaler and T.B. Jones, "Dielectrophoretic spectra of single cells determined by feedback-controlled levitation", Biophys. J., 57 (1990) 173-182.
5. K.V.I.S. Kaler, J-P. Xie, T.B. Jones and R. Paul, "Dual frequency dielectrophoretic levitation of canola plant protoplasts", Biophys. J., 63 (1992) 58-69.
6. J. Gimsa, T. Müller, T. Schnelle and G. Fuhr, "Dielectric spectroscopy of single human erythrocytes at physiological ionic strength: dispersion of the cytoplasm", Biophys. J., 71(1996) 495-506.
7. P. Gascoyne, X. Wang, Y. Huang, and F. Becker, "Dielectrophoretic separation of cancer cells from blood", IEEE Proceedings 1995, 1366-1373
8. Y. Huang, X.B. Wang, R. Hölzel, F. Becker, P. Gascoyne, "Electrorotational studies of the cytoplasmic dielectric properties of friend murine erythroleukaemia cells", Phys. Med. Biol. 40 (1995) 1789-1806.
9. X-B. Wang, Y. Huang, P.R.C. Gascoyne, F.F. Becker, R. Hölzel and R. Pethig, "Changes in friend murine erythroleukaemia cell membranes during induced differentiation determined by electrorotation" Bochim Biophys. Acta, 1193 (1994) 330-344.

10. W.M.Arnold, H.P. Schwan and U. Zimmermann, "Surface conductance and other properties of latex particles measured by electrorotation", J. Phys. Chem. 91 (1987) 5093-5098.

11. T.N. Tombs, The effect of adsorbed water on the polarization of individual glass particles suspended in silicone oil (a model electrorheological fluid), Ph.D. Thesis, University of Rochester (1992).

12. M. Washizu, O. Kurosawa, I. Arai and S. Suzuki and N. Shimamoto, " Application of electrostatic stretch and positioning of DNA", Proc. of IEEE/IAS annual meeting, Toronto, Canada (1993) 1629-1637.

13. M. Washizu, and O. Kurosawa, "Electrostatic manipulation of DNA in microfabricated structures", IEEE Trans. IA Vol. 26 (1990) 1165-1172.

14. J. Cheng, E.L. Sheldon, L. Wu, A. Uribe, L.O. Gerrue, J Carrino, M. J. Heller and J. P. O'Connell, "Preparation and hybridization analysis of DNA/RNA from E. coli on microfabricated bioelectronic chips", 16 (1998) 541-546.

15. G. Fuhr, W.M. Arnold, R. Hagedorn, T. Müller, W. Benecke, B. Wagner and U. Zimmermann, "Levitation, holding, and rotation of cells within traps made by high - frequency fields", Biochimica et Biophysica Acta, 1108 (1992) 215-223.

16. X-B. Wang, Y. Huang, P. Gascoyne and F. Becker, "Dielectrophoretic manipulation of particles", IEEE Proceedings, 1358-1365, 1995.

17. T. Müller, A. Gerardino, T. Schnell, S. Shirley, F. Bordoni, G.D. Gesperis, L. Leoni and G. Fuhr, "Trapping of micrometer and sub-micrometer particles by high frequency electric fields and hydrodynamic forces", J. Phys. D: Appl. Phys., 29(1996) 340-349.

18. A. Docoslis, N. Kalogerakis, L.A. Behie and K.V.I.S. Kaler, "A novel dielectrophoresis-based device for the selective retention of viable cells in cell culture media", Biotech. and Bioeng., 54(3) (1997) 239-250.

19. L. Hartley, K.V.I.S. Kaler, J. Luo and R. Paul, "Discrete planar electrode dielectrophoresis systems", Canadian Conf. On Elec. and Comp. Eng., St. Johns, Newfoundland., (1997) 185-188.

20. T.B. Jones, "Cusped electrostatic fields for dielectrophoretic levitation", J. of Electrostatics 11 (1981) 85-95.

21. M. Washizu and T.B. Jones, "Multipolar dielectrophorectic force calculations", J. of Electrostatics, 33 (1994) 187-198.

22. T.B. Jones and M. Washizu, "Multipolar dielectrophoretic and electrorotation theory", J. Electrostatics 37 (1996) 121-134.

23. M. Washizu and T.B. Jones, "Equilibria and dynamics of DEP-levitated particles: Multipolar Theory", J. Electrostatics 33 (1994) 199-212.

24. M. Washizu, T.B. Jones and K.V.I.S. Kaler, "Higher-order dielectrophoretic field effects: levitation at a field null", Biochimica et Biophysica Acta, 1158 (1993) 40-46.

Figure Captions

Fig. 1a The planar point charge quadrupole model showing the location of the source charges +Q and -Q in the x-y plane at (0,b,0), (0,-b,0), (-b,0,0) and (b,0,0) respectively. A test particle of radius r, is shown located at (0,0,z) on the central axis of the quadrupole.

Fig. 1b Plot of the normalized axial force versus normalized height for spherical particles of various radii (5-25 μm), obtained numerically, is compared with the analytical point charge model force profile.

Fig. 2 Comparison of the axial force profile of the discrete planar quadrupole obtained numerically (X) with the approximate point charge analytical data for 1 μm Spheriglass®) particles (+) .A best-fit condition was obtained using b=124 μm and $q=2.76\times10^{-13}$ C in the analytical point charge model.

Fig. 3 Diagram showing the cross-sectional view of the quadrupole fluid integrated circuit chamber housing and other fluid circuit components used in this investigation.

Fig. 4 Top view of the quadrupole chiplet used in the levitation experiments. The planar quadrupole is comprised of 4-50 μm radius circular unpassivated chrome-gold electrodes. The respective electrode centers were located at $x = \pm 100\,\mu$m and $y = \pm 100\,\mu$m.

Fig. 5 Typical images of a microscopic particle passively levitated at different axial locations above the planar circular electrode quadrupole. Note, the collection of sub-micron sized contaminant particles on the surface of the levitated test particle.

Fig. 6 Experimentally obtained normalized axial DEP force profile data for **(a)** Spheriglass® particles and **(b)** polymethylmethacrylate particles of various radii. The solid line plots in each figure represents the circular planar quadrupole numerical results obtained for a similar 1 μm particle, with the quadrupole electrodes biased by ± 1V sources.

Fig. 7 Plots of the extracted radius (r_{ext}) versus levitation height (z) for various sized test particles of **(a)** Spheriglass® and **(b)** polymethylmethacrylate.

Table 1

	Spheriglass®	polymethylmethacrylate
ε_1	6.9	2.75
$K_2 = \frac{\varepsilon_2 - \varepsilon_1}{2\varepsilon_2 + 3\varepsilon_1}$	-0.288	-0.315
$\delta(\mathrm{kg/m^3})$	2200	1100

Figure 1a

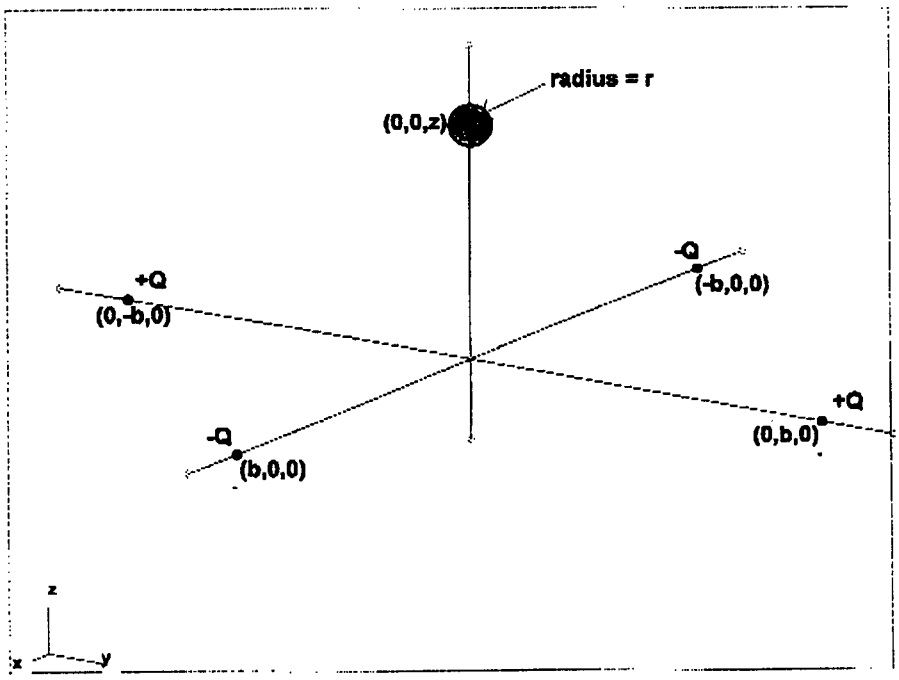

Figure 1b

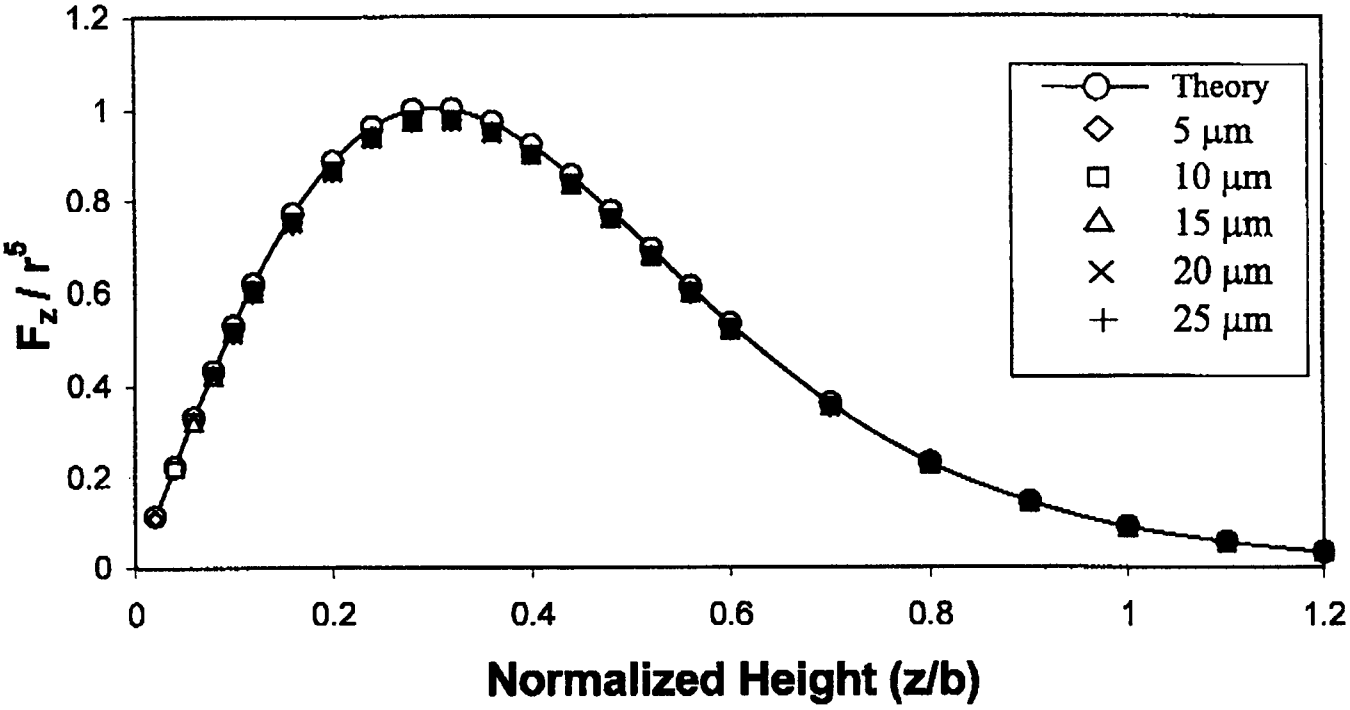
1.2
1
0.8
0.6
0.4
0.2
0
F_z / r^5
0
0.2
0.4
0.6
0.8
1
1.2
Normalized Height (z/b)
Theory
5 μm
10 μm
15 μm
20 μm
25 μm

Figure 2

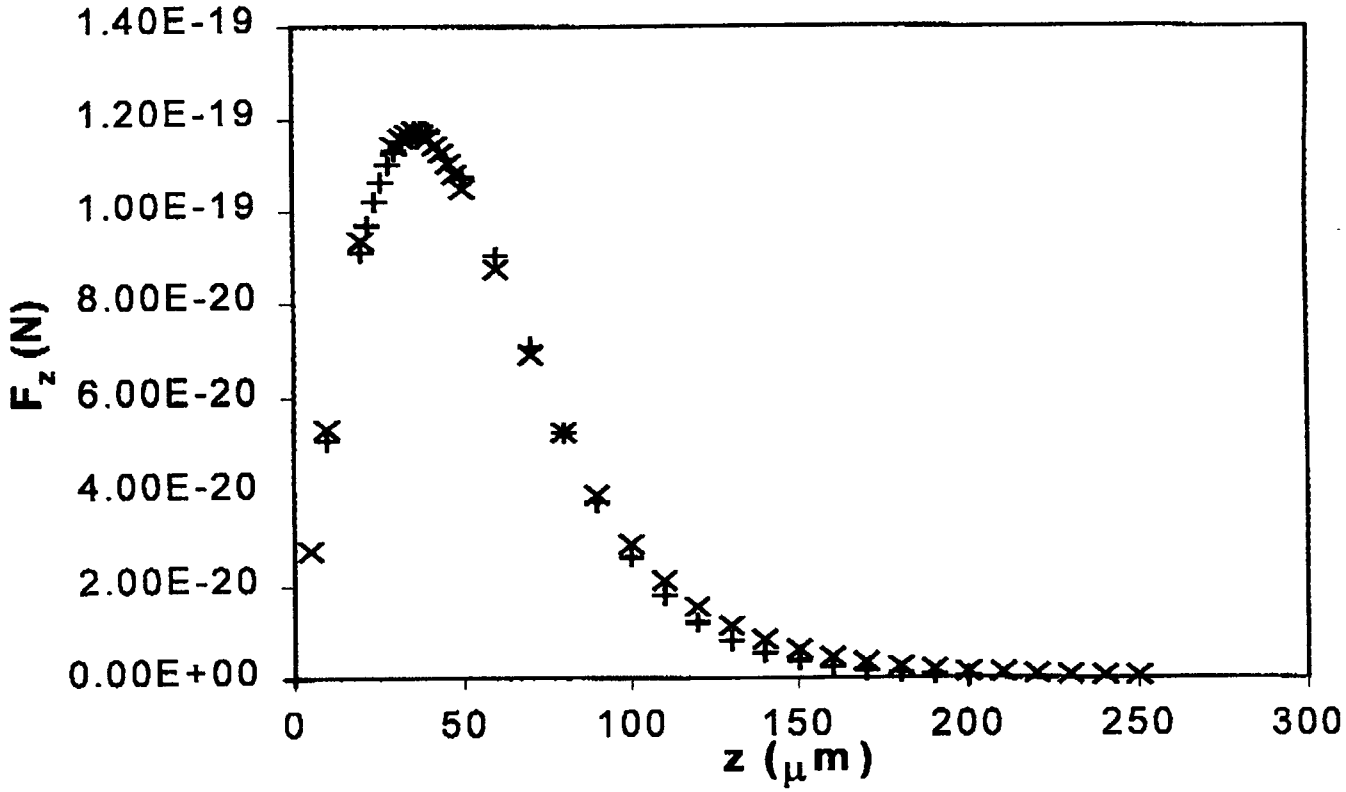
1.40E-19
1.20E-19
1.00E-19
8.00E-20
6.00E-20
4.00E-20
2.00E-20
0.00E+00
F_z (N)
0
50
100
150
200
250
300
z (μm)

Figure 3

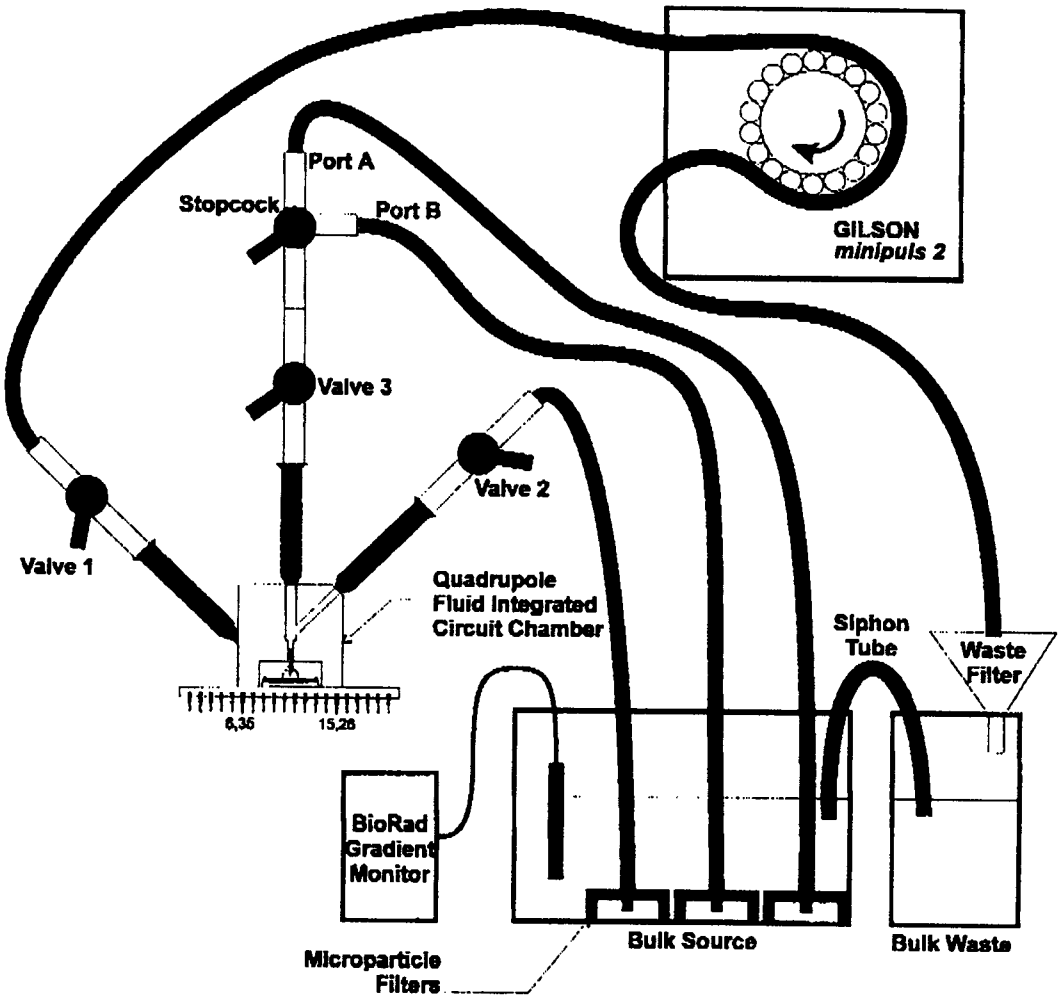
Port A
Stopcock
Port B
GILSON
minipuls 2
Valve 3
Valve 2
Valve 1
Quadrupole
Fluid Integrated
Circuit Chamber
6,35
15,26
Siphon
Tube
Waste
Filter
BioRad
Gradient
Monitor
Microparticle
Filters
Bulk Source
Bulk Waste

Figure 4

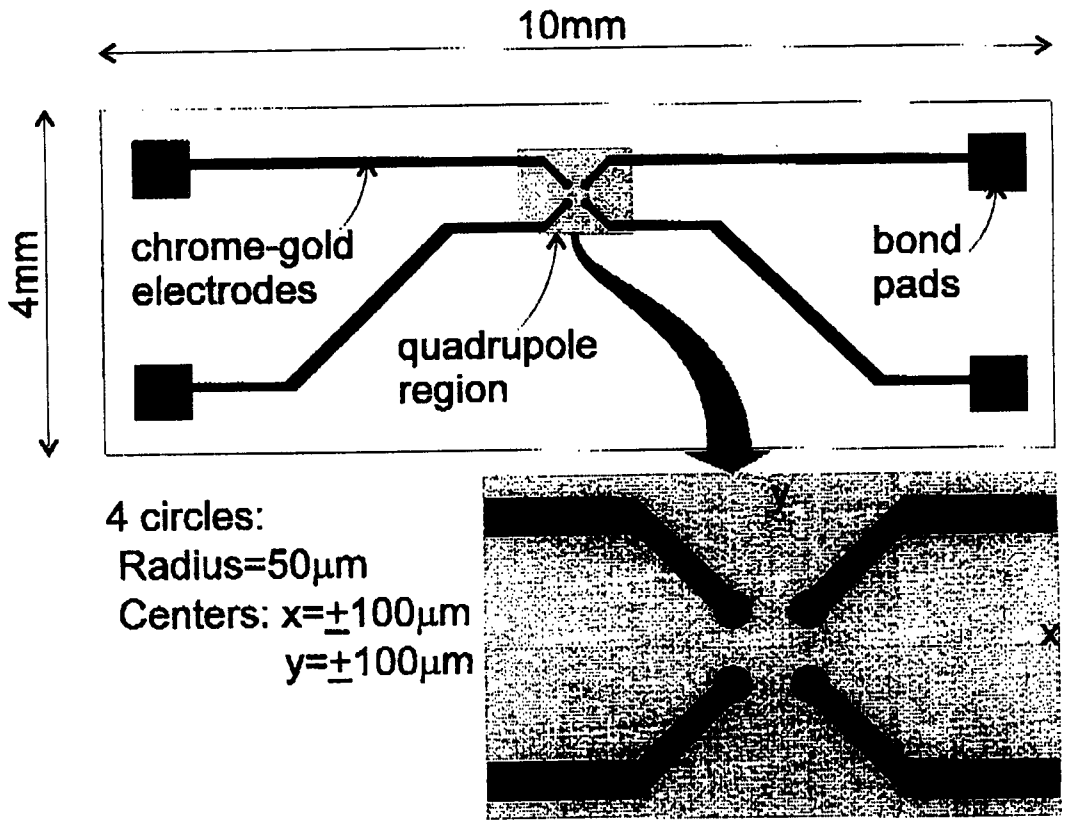
10mm
4mm
chrome-gold electrodes
quadrupole region
bond pads
4 circles:
Radius=50μm
Centers: x=±100μm
y=±100μm
y
x

Figure 5

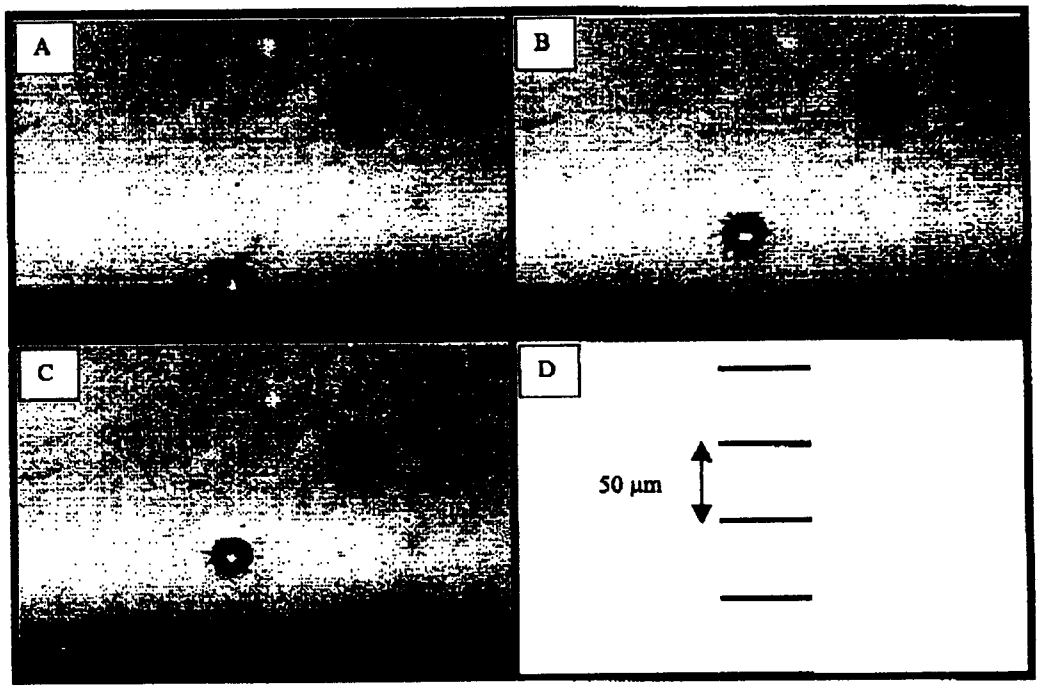

Figure 6a

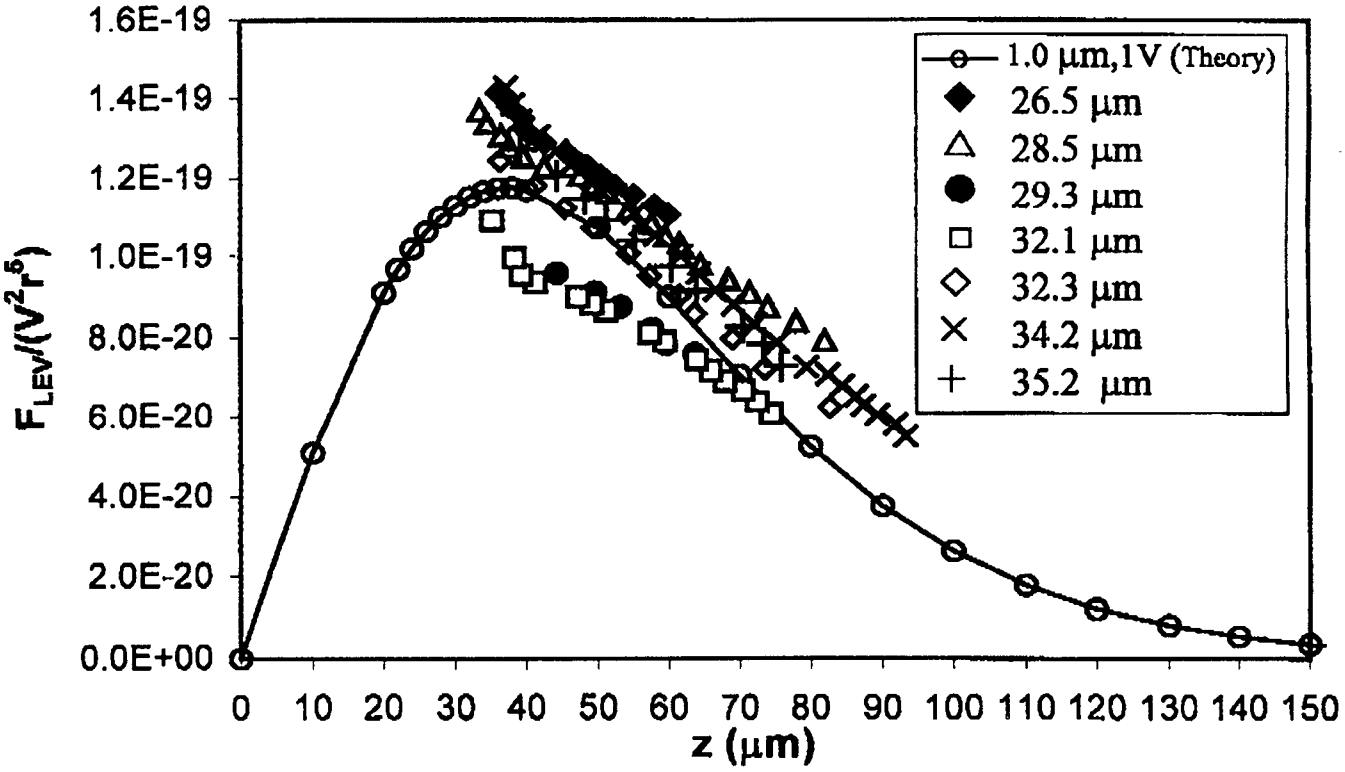
1.6E-19
1.4E-19
1.2E-19
1.0E-19
8.0E-20
6.0E-20
4.0E-20
2.0E-20
0.0E+00
$F_{LEV}/(V^2r^5)$
0
10
20
30
40
50
60
70
80
90
100
110
120
130
140
150
z (μm)
1.0 μm,1V (Theory)
26.5 μm
28.5 μm
29.3 μm
32.1 μm
32.3 μm
34.2 μm
35.2 μm

Figure 6b

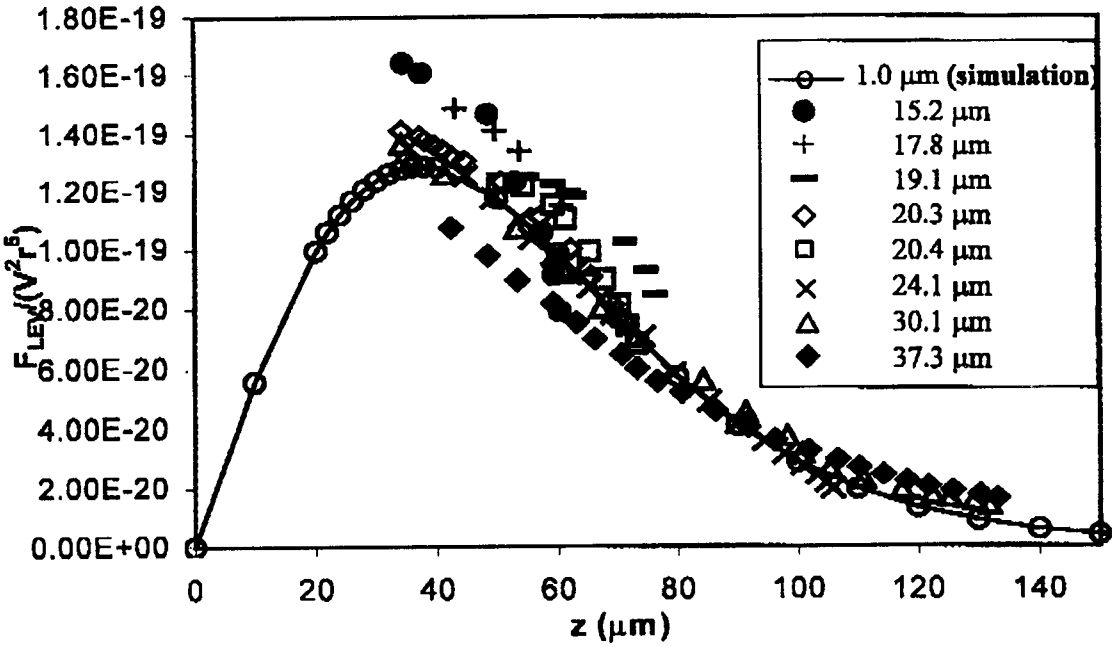
1.80E-19
1.60E-19
1.40E-19
1.20E-19
1.00E-19
8.00E-20
6.00E-20
4.00E-20
2.00E-20
0.00E+00
$F_{LEV}/(V^2r^5)$
0
20
40
60
80
100
120
140
z (μm)
1.0 μm (simulation)
15.2 μm
17.8 μm
19.1 μm
20.3 μm
20.4 μm
24.1 μm
30.1 μm
37.3 μm

Figure 7a

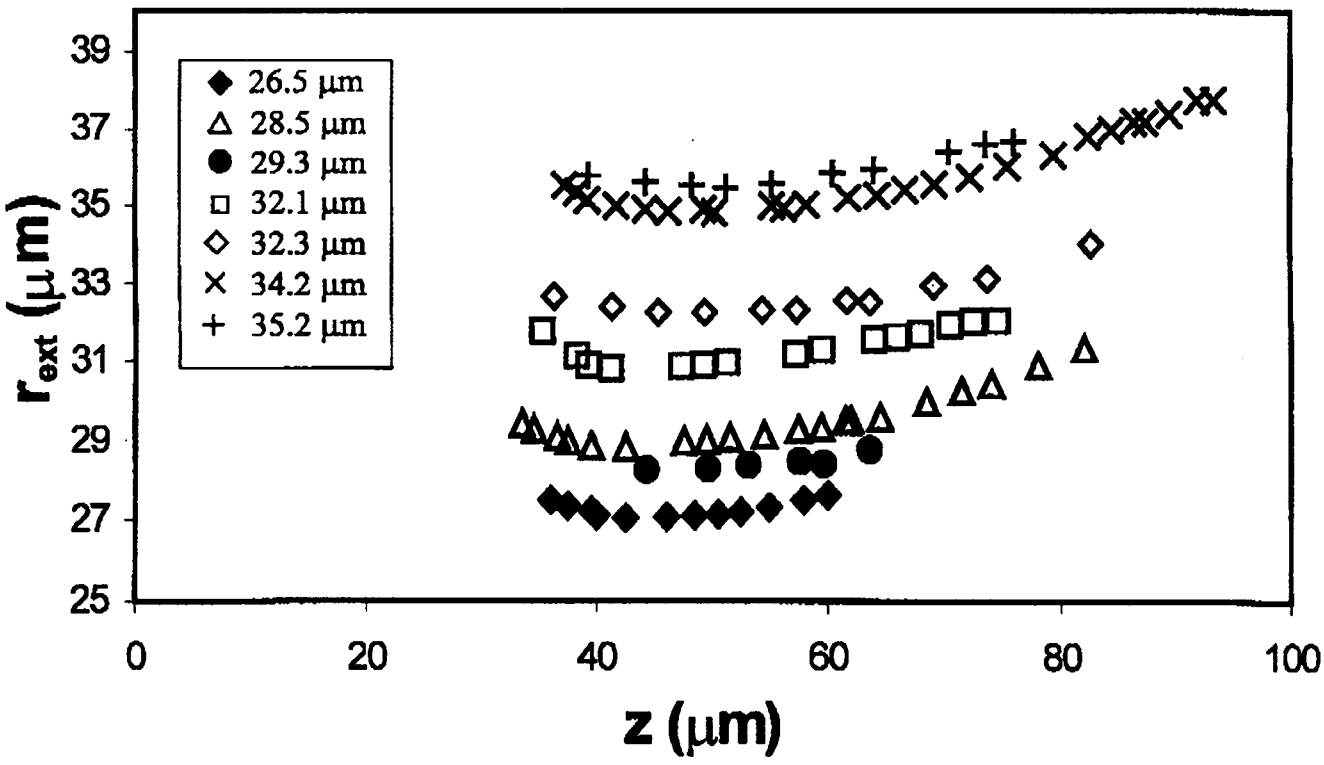
26.5 µm
28.5 µm
29.3 µm
32.1 µm
32.3 µm
34.2 µm
35.2 µm
r_{ext} (µm)
39
37
35
33
31
29
27
25
0
20
40
60
80
100
z (µm)

Figure 7b

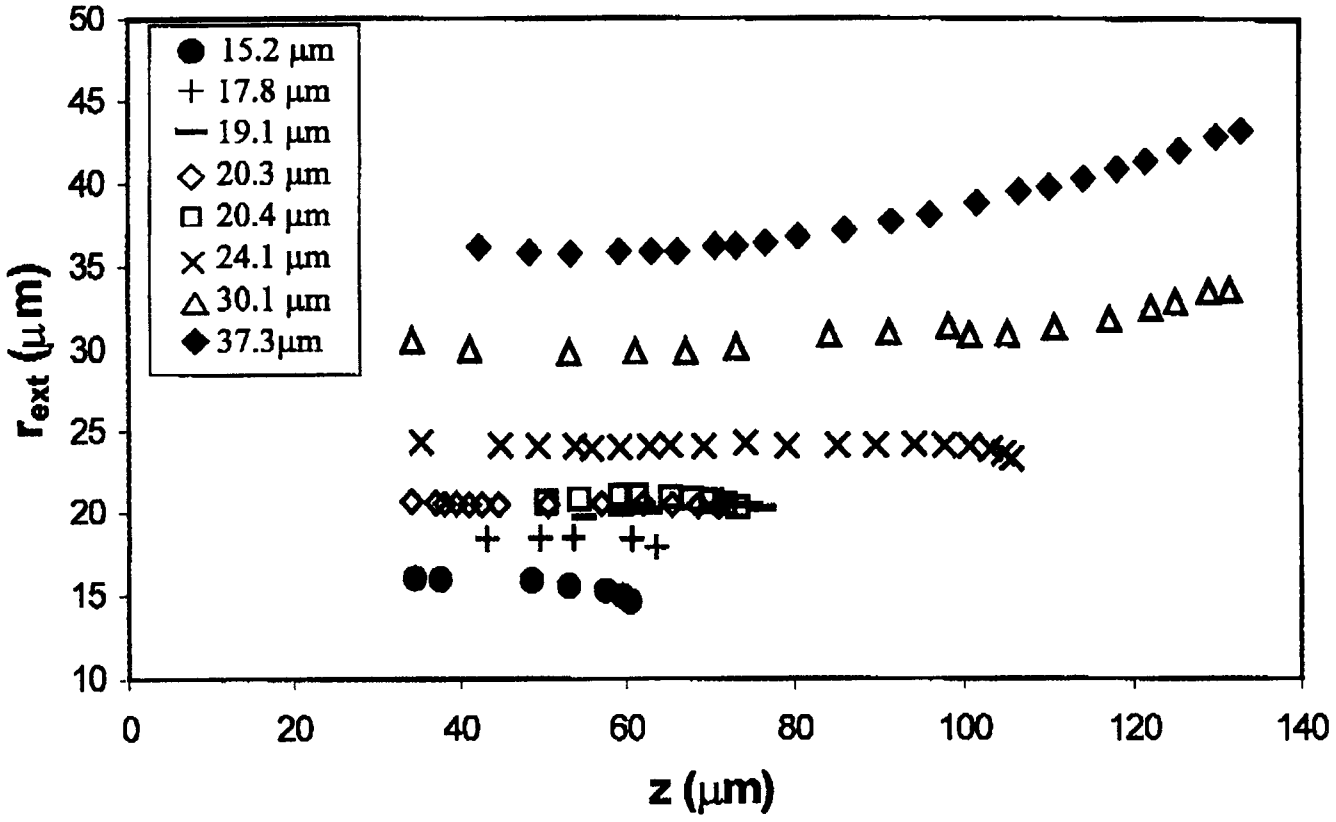
15.2 µm
17.8 µm
19.1 µm
20.3 µm
20.4 µm
24.1 µm
30.1 µm
37.3µm
r_ext (µm)
z (µm)
50
45
40
35
30
25
20
15
10
0
20
40
60
80
100
120
140